1 **Extracellular Electron Transfer Powers *Enterococcus faecalis* Biofilm Metabolism**

2 **Running Title: Iron promotes biofilm growth and EET in *E. faecalis***

3 Damien Keogh[1#], Ling Ning Lam[1,2#], Lucinda E. Doyle[1,3], Artur Matysik[1], Shruti Pavagadhi[4],

4 Shivshankar Umashankar[4], Jennifer L. Dale[5], Chris B. Boothroyd[6], Gary M. Dunny[5], Sanjay

5 Swarup[4,7], Rohan B. H. Williams[4], Enrico Marsili[1,8], and Kimberly A. Kline[1,2,*]

6 [1]Singapore Centre for Environmental Life Science Engineering, Nanyang Technological

7 University, 60 Nanyang Drive, Singapore 637551

8 [2]School of Biological Sciences, Nanyang Technological University, 60 Nanyang Drive,

9 Singapore 637551

10 [3]Interdisciplinary Graduate School, Nanyang Technological University, Singapore 639798

11 [4]Singapore Centre for Environmental Life Science Engineering, National University of

12 Singapore, 28 Medical Drive, Singapore, 114756

13 [5]Department of Microbiology, University of Minnesota Medical School, Minneapolis,

14 Minnesota, USA

15 [6]School of Materials Science and Engineering, Nanyang Technological University, 50

16 Nanyang Avenue, Singapore 639798

17 [7]Department of Biological Sciences, National University of Singapore, 14 Science Drive 4,

18 Singapore 117543

19 [8]School of Chemical and Biomedical Engineering, Nanyang Technological University, 62

20 Nanyang Drive, Singapore 637459

21 [#]Equal contribution

22   *Correspondence: kkline@ntu.edu.sg

23   **Classification:** Biological Sciences – Microbiology

Abstract

Enterococci are important human commensals and significant opportunistic pathogens associated with endocarditis, urinary tract infections, wound and surgical site infections, and medical device associated infections. These infections often become chronic upon the formation of biofilm. The biofilm matrix establishes properties that distinguish this state from free-living bacterial cells and increase tolerance to antimicrobial interventions. The metabolic versatility of the Enterococci is reflected in the diversity and complexity of environments and communities in which they thrive. Understanding metabolic factors governing colonization and persistence in different host niches can reveal factors influencing the transition from commensal to opportunistic pathogen. Here, we report a new form of iron-dependent metabolism for *Enterococcus faecalis* where, in the absence of heme, respiration components can be utilised for extracellular electron transfer (EET). Iron augments *E. faecalis* biofilm growth and generates alterations in biofilm matrix, cell spatial distribution, and biofilm matrix properties. We identify the genes involved in iron-augmented biofilm growth and show that it occurs by promoting EET to iron within biofilm.

41 **Significance**

42 Bacterial metabolic versatility is often key in dictating the outcome of host-pathogen

43 interactions, yet determinants of metabolic shifts are difficult to resolve. The bacterial biofilm

44 matrix provides the structural and functional support that distinguishes this state from free-

45 living bacterial cells. Here, we show that the biofilm matrix provides access to resources

46 necessary for metabolism and growth which are otherwise inaccessible in the planktonic

47 state. Our data shows that in the absence of heme, components of *Enterococcus faecalis*

48 respiration (l-lactate dehydrogenase and acetaldehyde dehydrogenase) may function as

49 initiators of EET through the cytoplasmic membrane quinone pool and utilize matrix-

50 associated iron to carry out EET. The presence of iron resources within the biofilm matrix

51 leads to enhanced biofilm growth.

52

Introduction

Human colonization by Enterococci initiates immediately at birth via gastrointestinal inoculation from maternal sources, diet, and the environment (1). *Enterococcus faecalis* represents a significant proportion of this early Enterococcal population and remains a stable member of the community throughout life (1). In the gastrointestinal tract, Enterococci are present in the lumen as well as in more specialized niches in the physicochemically complex mucus epithelial layer and epithelial crypts in the small intestine (2).

Bacterial biofilms contribute to host health and disease, and are complex systems that rely on the biofilm matrix to provide the structural and functional properties that distinguish this state from free-living bacterial cells (3). The dynamics of biofilm formation are dependent on many factors such as nutrient availability, environmental stress, social competition, and the generation of extracellular matrix materials. These extracellular polymeric substances provide the architecture surrounding the bacterial cells enabling emergent properties such as resource capture, tolerance to antimicrobial compounds, cooperation or competition, and localized gradients. Infections can become chronic through the development of biofilm. Antimicrobial interventions and colonization by multidrug resistant bacteria can influence endogenous gut microbiome diversity. In both adults and neonates in intensive care settings, gastrointestinal perturbations can result in the replacement of the endogenous Enterococci with aminoglycoside- or vancomycin-resistant Enterococci (4-6). Enterococci are also opportunistic pathogens associated with surgical site and wound infections, bacteraemia, urinary tract infections (UTI), catheter-associated UTI (CAUTI), and endocarditis (7-10). These infections can become chronic through the development of biofilm which is inherently more tolerant to antimicrobial therapies and immune clearance, a problem compounded by multidrug resistant Enterococci in healthcare settings.

5

77   The lactic acid bacteria, which include Enterococci, use an electron transport chain for

78   aerobic respiration when external heme is provided or, alternatively, can perform

79   fermentation in the absence of heme. *E. faecalis* does not synthesize heme *de novo* and

80   therefore lacks porphyrin rings required for cytochrome *bd* activity during cellular respiration

81   (11, 12). Similar to other members of the lactic acid bacterial group, *E. faecalis* does not have

82   a major growth requirement for nutritional iron, with manganese instead being used as the

83   essential cofactor for cellular processes (13-16). *E. faecalis* is also remarkably resistant to

84   oxidative stress from O_2^-, hydroxyl radicals ($OH^\cdot$), and hydrogen peroxide (H_2O_2) sources

85   from incomplete reduction of oxygen during respiration; from the oxidative action of host

86   immune cells; or that arise during the Fenton reaction (17, 18). These findings suggest that *E.*

87   *faecalis* may be able to withstand iron at concentrations which are typically toxic to most

88   bacterial species. In human serum, free iron is far below the 10^{-7} to 10^{-5} M optimal range

89   required to support the growth of most bacteria (19). However, iron availability in the host

90   can vary. Disease states such as haemochromatosis and thalassemia disrupt homeostasis and

91   cause excess iron accumulation (20, 21). Iron oxides have been detected in human spleens

92   and the iron concentration of the gastrointestinal tract is sufficient to support bacterial growth

93   (22, 23). Moreover, *E. faecalis* is tolerant to conditions of significant iron limitation and high

94   oxidative stress (13-18, 24, 25).

95   In this study, we hypothesize that the ability to withstand higher iron concentrations provides

96   a metabolic advantage to *E. faecalis*. We combine biofilm studies, transmission electron

97   microscopy (TEM), confocal laser scanning microscopy (CLSM), forward genetics, and

98   chronocoulometry to reveal a novel mode of biofilm-specific metabolism in *E. faecalis* where

99   the biofilm matrix harbours iron sinks involved in extracellular electron transport to support

100   biofilm growth. Understanding the metabolic factors that promote colonization and biofilm

101   formation in different environmental conditions may inform mechanisms governing the

102   switch from commensal to opportunistic pathogen and the spread of multidrug resistant

103   Enterococci in a number of ecological reservoirs.

Results

104

105 **Iron supplementation promotes *Enterococcus faecalis* biofilm growth and alters biofilm**

106 **matrix and matrix properties.** To understand the influence of iron on *E. faecalis* biofilm,

107 we evaluated biofilm growth using ferric chloride ($FeCl_3$) enriched medium. We analyzed

108 biofilm by confocal laser scanning microscopy (CLSM) in the absence (normal) and presence

109 (supplemented) of additional $FeCl_3$ in a flow cell biofilm system. Using a GFP-expressing *E.*

110 *faecalis* strain, we observed augmented biofilm accumulation as early as 8 hours in medium

111 supplemented with 0.2 mM $FeCl_3$ compared to normal medium (Fig. 1a). Iron-enhanced

112 biofilm growth continued for 18 hr, in contrast to the thinner normal biofilm. Iron

113 supplementation did not augment *E. faecalis* growth in planktonic culture (Fig. S1) indicating

114 that the promotion of *E. faecalis* growth is a biofilm specific phenotype. For detailed

115 visualization of *E. faecalis* cell distribution and biofilm architecture properties, we created 3D

116 reconstructions of high magnification CLSM stacks (Fig. 1b). At 18 hr, 37 ^{o}C *E. faecalis*

117 biofilm forms a flat monolayer in the normal medium as reported previously (26, 27). By

118 contrast, *E. faecalis* biofilm is thicker and the bacterial cells are distributed throughout the

119 iron supplemented biofilm. Increased biofilm thickness indicates an expansion in biofilm

120 matrix in the supplemented medium suggesting a role for the matrix in iron-enhanced

121 biofilms. We further hypothesized that *E. faecalis* gains a metabolic advantage by the

122 supplementation of iron which in turn affects growth rate. We reasoned that by reducing the

123 temperature we could slow the *E. faecalis* growth rate and possibly modulate the dependence

124 on iron supplementation. At 120 hr, *E. faecalis* grown at 22 ^{o}C forms a sparse monolayer

125 biofilm in normal medium; however, the biofilm expands to a depth of greater than 24 μm

126 (the image resolution limit of CSLM) and increased cell density in iron supplemented

127 medium. To evaluate morphological changes in *E. faecalis* cells or the biofilm matrix, we

128 analyzed biofilm cells grown in flow chambers by transmission electron microscopy (TEM).

129   We observed typical diplococcal *E. faecalis* in the normal biofilm cells with an abundance of

130   extracellular fibrous material in the matrix (Fig. 2a,b,c). Constituents of the *E. faecalis*

131   biofilm matrix are not well-understood; however, *E. faecalis* can actively secrete eDNA in

132   biofilms, and DNAse treatment can disperse *E. faecalis* biofilms suggesting eDNA is a major

133   component of the matrix (28-30). The TEM images of the iron supplemented biofilm are

134   similar to normal biofilm (Fig. 2a,b,c), with the exception of electron-dense particles

135   associated with the extracellular fibrous matrix material (Fig. 2d,e,f). Using energy-dispersive

136   X-ray spectroscopy (EDS) in a TEM to analyse the same samples, we demonstrated the

137   extracellular electron-dense particles to be enriched in iron (Fig 2g-m) and hypothesize that

138   these iron deposits together with the increased biomass observed by CSLM are important for

139   augmented *E. faecalis* biofilm formation.

140   **Iron-induced *Enterococcus faecalis* growth is biofilm specific and iron availability**

141   **impacts the metallome.** To determine if redox-active metals other than iron could also

142   augment *E. faecalis* biofilm formation, we performed biofilm assays with quantification via

143   crystal violet (CV) staining in microtitre plate format to increase throughput (31). In all

144   biofilm assays we included abiotic media controls with metals supplemented to monitor metal

145   precipitation and found that no metals fell out of solution at the concentrations tested in these

146   assays (see Material and Methods – Biofilm Assays, Fig S1). Consistent with *E. faecalis*

147   biofilm augmentation observed when grown in flow cells with 0.2 mM $FeCl_3$ supplemented

148   (Fig. 1a,b), $FeCl_3$ enriched medium facilitated enhanced *E. faecalis* biofilm growth over time

149   (0 to 120 hr) compared to the normal medium (Fig. 3a). The biofilm increased significantly in

150   response to increasing $FeCl_3$ supplementation with 0.5 to 2 mM providing the optimal

151   concentration range in this assay. Above these concentrations, growth was also enhanced but

152   not as significantly compared to the non-supplemented control. We next investigated the

153   capacity of different metal species for enhanced *E. faecalis* biofilm accumulation and found

154   that supplementation with ferrous sulfate ($FeSO_4$) or ferric sulfate ($Fe_2(SO_4)_3$) also increased

155   *E. faecalis* biofilm growth; whereas ferric citrate, magnesium chloride, zinc chloride, or

156   copper chloride had negligible influence on *E. faecalis* biofilm accumulation (Fig 3b).

157   Manganese chloride had a modest augmenting effect on biofilm formation. Heme

158   supplementation at concentrations from 0 to 150 µM also significantly promoted biofilm

159   accumulation and is likely the result of enhanced activity in cytochrome *bd* since heme

160   functions as a cofactor for this enzyme and drives *E. faecalis* to aerobic respiration (32).

161   TEM analysis (Fig. 2d, e, f) revealed iron deposits in the extracellular biofilm matrix of the

162   iron supplemented cultures, whereas no extracellular deposits were observed for biofilms

163   supplemented with heme (Fig S3). We therefore hypothesized that iron concentrations in the

164   *E. faecalis* intracellular metallome would remain stable between the normal and iron

165   supplemented cultures. We used inductively coupled plasma mass spectrometry (ICP-MS) to

166   quantify the intracellular metallome of *E. faecalis* in the absence (normal) and presence

167   (supplemented) of $FeCl_3$ supplementation (Fig. 3d, Table S1). The overall intracellular metal

168   content when grown in iron-supplemented medium (3125 ppb) was actually lower than when

169   grown in the normal medium (4641 ppb). Iron was present at 675 ppb in the supplemented

170   samples and 20 ppb in the normal samples. However, the increase in intracellular iron

171   concentration was coincident with a decrease in intracellular cobalt and zinc when *E. faecalis*

172   was grown in iron-supplemented medium. Together, this data suggested that iron was

173   substituting for other metals in the supplemented medium and that the substitution was likely

174   to be functionally balanced. Iron, cobalt, and zinc are transition metals that can function as

175   interchangeable ions and can compete with iron for binding to metalloproteins (33). We

176   hypothesized that identifying genes involved in metal acquisition would help determine if

177   intracellular iron was important for iron-enhanced biofilm growth. We selected 21 mutants of

178   uncharacterized *E. faecalis* membrane transport or regulation systems, with homology to

179   previously characterized metal-associated proteins in other bacteria, from a sequenced

180   mariner transposon library and measured intracellular metal content by ICP-MS (Table S2,

181   S3, S4) (34). These mutants did not have significant changes in intracellular iron

182   concentration in the normal or supplemented medium, with only cobalt and zinc displaying

183   significant changes in some of the mutants and only in the normal medium (Table S2).

184   Because bacterial iron transport systems are generally expressed under iron limitation, we

185   tested these mutants in an iron chelated medium where *E. faecalis* planktonic growth has

186   previously been shown to be growth limited (25). We detected an absence of intracellular

187   iron in 15 mutants under iron limited growth (Table S5) suggesting that these genes govern

188   iron acquisition and may only be active under conditions of low iron availability. Overall,

189   the ICP-MS analysis has demonstrated the modulation of the *E. faecalis* metallome when

190   cultured at different iron concentrations and identified systems involved in metal acquisition.

191   However, this study did not identify any systems involved in iron acquisition in the

192   supplemented medium suggesting that they are not involved or there is a large amount of

193   overlapping functionality in iron transport in *E. faecalis*. These findings support the

194   hypothesis that extracellular electron-dense particles are important for augmented *E. faecalis*

195   biofilm growth in the presence of iron.

196

197   **Components of *E. faecalis* metabolism contribute to iron-induced biofilm growth.** To

198   determine the mechanism underlying iron-enhanced *E. faecalis* biofilm, we screened a near-

199   saturated *E. faecalis* mariner transposon library for changes in biofilm formation in media

200   supplemented with 2 mM FeCl$_3$ (34). Using the CV biofilm assay, we screened the

201   transposon library for mutants displaying either loss or further enhancement of biofilm

202   growth (Fig. S4a). Mutants displaying altered biofilm growth in iron supplemented media

203   were also examined for alterations in planktonic growth in normal or supplemented media, to

11

204 eliminate mutants with general fitness defects (Fig. S4a). Because we were seeking factors

205 specifically involved in biofilm formation in excess iron, and not general biofilm factors, we

206 performed a secondary biofilm assay to exclude mutants that displayed altered biofilm in

207 both iron supplemented and normal medium (Fig. S4b-g). The final *E. faecalis* transposon

208 mutants that specifically altered biofilm formation in excess iron included *phoH*, *ldh1*, *trxB2*,

209 OG1RF_11340, OG1RF_10589, and an intergenic region (Table S6). The predicted functions

210 for all of the gene products were associated with metabolism functions and membrane

211 transport.

212

213 **Extracellular electron transfer to iron occurs in *E. faecalis* biofilm.** Dissimilatory metal-

214 reducing bacteria, such as *Shewanella* spp. and *Geobacter* spp., take advantage of

215 extracellular redox-active metals as terminal electron acceptors for respiration by EET (35,

216 36). *Shewanella* spp. and *Geobacter* spp. both have functional iron transport and regulation

217 systems for intracellular iron homeostasis (37, 38). EET can function by both direct electron

218 transfer (DET), which involves outer membrane c-type cytochromes (39) and mediated

219 electron transfer (MET), which avails of microbially produced redox mediators (40-43). Our

220 data indicate that genes involved in energy production, redox control, and membrane

221 transport contributed to iron-augmented biofilm formation (Table S2). We also observed iron

222 deposits in the biofilm matrix that surrounds the bacterial cell surfaces of iron-enhanced

223 biofilm (Fig. 2d, e, f, k, m). We therefore hypothesized that the extracellular iron associated

224 with *E. faecalis* biofilm matrix may function as electron sinks via either DET or MET during

225 biofilm metabolism, where Fe(III) is reduced to Fe(II) by *E. faecalis*. To test this, we used

226 chronocoulometry to measure EET of *E. faecalis* biofilms grown in electrochemical cells on a

227 carbon screen-printed electrode (SPE) maintained at high oxidative potential. In the case of

228 DET, extracellular Fe(III) would be reduced by *E. faecalis* and subsequently re-oxidized in

229 part by the electrode in order to regenerate it for further use as an electron acceptor by *E.*

230 *faecalis*. Alternatively, if the specific mode of EET was MET, we would detect iron acting as

231 a mediator/electron shuttle, carrying electrons extracellularly between *E. faecalis* and the

232 electrode. Electrons are only detected at the electrode surface, and as such any intracellular

233 iron reduction cannot be measured. Thus, in the case of either DET or MET,

234 chronocoulometry allows for the monitoring whether *E. faecalis* is capable of sustained EET

235 when oxidized iron was in its environment in real-time. Additionally, this electrochemical

236 technique measures the integral of current over time, i.e., the charge transferred to the

237 electrode over time (35). Chronocoulometry is commonly used to measure the electron

238 transfer process in redox systems (35, 44). In whole cell bioelectrochemical systems,

239 chronocoulometry is preferred over chronoamperometry to provide a quantitative measure of

240 charge transfer (45). Chronocoulometry was previously used to measure MET in

241 *Pseudomonas aeruginosa* (42). We observed that *E. faecalis* biofilms grew on the carbon

242 electrode (Fig S5a, b) and generated extracellular current in iron supplemented medium,

243 while all abiotic media controls and *E. faecalis* biofilms grown in normal medium did not

244 yield a current (Fig. 4a). Moreover, extracellular current generation was specific to the

245 addition of iron, because we observed no current upon the addition the other biofilm-

246 augmenting metals magnesium, manganese, or heme (Fig. S5c). We then tested the six

247 mutants identified through the transposon screen for the generation of extracellular current in

248 the supplemented medium. Two of the six mutants displayed significantly reduced current as

249 compared to the parental strain. These mutants contained transposon insertions in the genes

250 *ldh1* and OG1RF_11340 suggesting that l-lactate dehydrogenase and acetaldehyde

251 dehydrogenase were involved in extracellular electron transfer in *E. faecalis*.

252 Complementation studies could not be performed because all attempts to clone *ldh* or *adh* on

253 a plasmid *in trans* resulted in an accumulation of mutations preventing the expression of the

254   gene product, presumably due to cytotoxic effects of heterologous metabolic enzyme

255   expression in *E. coli*. To validate that extracellular iron was required as either an electron

256   acceptor (DET) or electron mediator/shuttle (MET), we spiked the electrochemical cell with

257   the chelator 2,2ꞌdipyridyl to sequester iron. In the presence of iron chelation, we observed a

258   significant reduction in current (Fig. 4b), demonstrating that extracellular iron was

259   instrumental to the process of EET.

260   Taken together, our results establish a model for *E. faecalis* biofilm metabolism where EET

261   using biofilm matrix associated iron supports biofilm growth (Fig. 5). We propose that in the

262   absence of heme, as was the condition in this study, where cytochrome *bd* would be non-

263   functional for aerobic respiration, fermentation end-products such as lactate and acetaldehyde

264   can be used as substrates by l-lactate dehydrogenase (LHD) and acetaldehyde dehydrogenase

265   (ADH) to generate a modification of the electron transport chain. We suggest that these

266   dehydrogenases may act as electron donors transferring electrons to the cytoplasmic

267   membrane quinone (dimethyl menaquinone) pool and ultimately use iron in the biofilm

268   matrix to carry out EET.

269 **Discussion**

270 In this study, we characterize a new form of *E. faecalis* metabolism where EET utilising iron

271 results in superior biofilm growth. Understanding the diversity of metabolic possibilities may

272 be important for understanding how *E. faecalis* colonizes different niches such as the human

273 gastrointestinal tract which harbours an abundance of iron (46). Iron rich niches also occur in

274 disease states such as haemochromatosis and thalassemia where iron homeostasis is defective

275 (20, 21). *E. faecalis* is a significant opportunistic pathogen and biofilm development

276 strengthens its tolerance to antimicrobial therapies and immune clearance (7-10).

277 Enterococcal metabolic versatility supports its survival in diverse and complex environments

278 and communities, thus increasing the possibility of dissemination to new niches when iron is

279 present (47). Communities within biofilm are dependent on nutrient and oxygen gradients,

280 cell-to-cell contact and communication, and metabolic cooperation (3). Matrix-associated

281 iron deposits are accessible simultaneously by a number of *E. faecalis* cells and can therefore

282 function as a shared biofilm community resource to enhance biofilm growth.

283 Our findings demonstrate that *E. faecalis* is electroactive and can utilize EET using iron in

284 the biofilm matrix, via either DET or MET, to enhance biofilm growth. In our model,

285 glycolysis and fermentation proceed prior to EET-dependent respiration to generate the end-

286 product substrates for dehydrogenases acting as electron donors. DET would occur by a

287 mechanism where extracellular iron can be reduced and become an iron sink for electrons of

288 the respiratory electron transport chain. Part of this reduced iron is then reoxidized at the

289 electrode, serving as an electron mediator/shuttle. While further studies are needed to resolve

290 the details of the EET mechanism to iron and to the electrode, these findings extend the

291 current knowledge regarding the extent of EET-capable bacterial species and environments,

292 which are primarily viewed in the context of energy recovery in systems such as microbial

293 fuel cells (36). The characterization of a role for EET in *E. faecalis* metabolism furthers our

294   understanding of possible mechanisms governing colonization and persistence in host niches.

295   Previous studies have demonstrated cell surface-associated oxidation/reduction potential and

296   capacity to utilize exogenously added soluble redox mediators in some Gram-positive

297   bacteria (48, 49). By contrast, we use chronocoulometry to quantify iron-related metabolism

298   in real time, as seen by the sustained generation of an electron flow by the biofilm, leading to

299   augmented biofilm growth. Chronocoulometry quantifies charge transfer at the electrode

300   surface and as such can only detect extracellular iron reduction. In addition,

301   chronocoulometry can show bacterial that derived extracellular electron transfer is

302   sustainable, whereas other commonly used techniques such as cyclic voltammetry can only

303   demonstrate the presence of redox-active moieties on the cell surface and cannot predict

304   whether sustained electron transfer will be possible.

305   *E. faecalis* and other lactic acid bacteria (LAB) encode the components necessary for aerobic

306   respiration metabolism (50). These are: (1) NADH dehydrogenases functioning as electron

307   donors, (2) a quinone pool to transfer electrons to (3) the terminal electron acceptor complex

308   cytochrome oxidase (51). The *E. faecalis* cytochrome *bd* enzyme can only use oxygen as a

309   terminal electron acceptor when exogenous sources of its co-factor heme are available (11,

310   52). *E. faecalis* does not synthesise porphyrin and in the absence of heme relies on

311   fermentation. Our experimental assays mimic the absence of heme as this is absent from the

312   growth medium. Our bioelectrochemical data suggests that *E. faecalis* l-lactate and

313   acetaldehyde dehydrogenases function as electron donors for EET to biofilm matrix

314   associated iron sinks. Dehydrogenases transfer hydride from one substrate to another in a

315   reversible reaction that relies on the interconversion of NADH and NAD^+. Previous studies

316   suggest that, in contrast to most bacterial species that rely on the tricarboxylic acid cycle

317   (TCA) to produce NADH, LAB instead rely on fermentation for its production (53).

318   Fermentation therefore is a necessary metabolic phase prior to the use of EET to support

319   biofilm metabolism. In *Lactococcus lactis*, a fermenting LAB strain, activation of respiration

320   metabolism in the absence of heme and oxygen reduction occurs by copper reduction via the

321   menaquinone pool (54). This supports our finding that extracellular iron functioning as a

322   electron acceptor and/or mediator can activate respiration metabolism in the absence of heme

323   and cytochrome *bd* activity.

324   Our biofilm data demonstrates an iron-specific *E. faecalis* enhanced biofilm growth response,

325   with only $FeCl_3$, heme, $FeSO_4$ and $Fe_2(SO_4)_3$ stimulating the response. Heme availability

326   enables respiration through cytochrome *bd* activity in the presence of oxygen (32). $FeSO_4$ and

327    $Fe_2(SO_4)_3$ are more labile to oxidative changes and precipitation, required for DET-driven

328   iron reduction, than the more soluble ferric citrate which does not enhance biofilm growth.

329   While flow cell biofilm generated enhanced growth at 0.2 mM $FeCl_3$, the static biofilm

330   assays only detected enhanced growth from 0.5 to 2 mM $FeCl_3$ supplementation.

331   *E. faecalis* can flourish in iron limited environments and tolerate oxidative stress which can

332   be induced by a high iron environment, contrasting with many other bacterial species where

333   iron is an essential growth nutrient and requires strict iron homeostasis (55). Nonetheless, our

334   ICP-MS analysis shows that iron represents a large proportion of the *E. faecalis* metallome

335   under normal conditions. The modulation of the *E. faecalis* metallome with changes in

336   conditions of either iron limitation or abundance suggests alternative roles for this metal. The

337   absence of detectable iron in the *E. faecalis* mutants with disruptions in genes predicted to

338   encode iron transport and regulatory components, analyzed by ICP-MS under iron limitation,

339   suggests these gene products function in iron acquisition. Previous transcriptomic studies

340   propose roles for *E. faecalis* transport systems in iron acquisition; however our ICP-MS

341   analysis is the first functional characterization of these systems (56, 57). Manganese has been

342   reported to substitute for iron as a cofactor in essential cellular reactions of LAB species,

343   however our data demonstrate that iron represents a greater proportion of the *E. faecalis*

344   metallome than manganese in normal and supplemented conditions (14, 15). The ICP-MS

345   analysis equally highlights that a number of other metals such as zinc, potassium, and

346   magnesium are abundant. Cobalt and zinc are important metals for bacterial growth and we

347   have identified a number of genes governing cobalt and zinc utilization in *E. faecalis* (58).

348   While the intracellular iron levels in the iron supplemented medium was greater than that of

349   the normal condition, no iron transport systems could be identified under these conditions.

350   The absence of detectable transport systems by ICP-MS and the presence of extracellular

351   electron dense deposits in our TEM data suggests that our model of EET would favour DET

352   rather than MET. However, overlapping functionality in nutrient transport is a common

353   strategy for bacteria so single gene mutations may not be sufficient in this condition.

354   Intracellular storage of iron may be strategic in anticipation of acceptor-limited conditions

355   where this metal can be deposited extracellularly.

356   Colonization and persistence in host niches require adaptability in the exploitation of

357   available resources for energy production and growth. *E. faecalis* is an important human

358   commensal and opportunistic pathogen present in the gastrointestinal tract throughout life.

359   Our work highlights a new form of metabolism where, in the absence of heme, components

360   of respiration can be utilized for EET using extracellular iron. This deeper understanding of

361   mechanisms governing biofilm metabolism in human and clinically relevant bacterial species

362   will enhance approaches to modify or eradicate these reservoirs.

363

364 **Materials and Methods**

365 **Bacterial Strains and Growth Conditions.** *Enterococcus faecalis* OG1RF

366 (ATCC47077)(59) was grown in Brain Heart Infusion broth (BHI) and cultured at 37 ^{o}C

367 under static conditions. *E. faecalis* SD234 is an OG1RF strain derivative harbouring a

368 constitutively expressed *gfp* gene (60). Overnight cultures were normalized to 2-4x10^8

369 CFU/ml in phosphate buffered saline (PBS), equivalent to OD_{600nm} 0.7 for *E. faecalis*. For

370 planktonic and biofilm assays, bacteria were cultured at 37 ^{o}C (under 200 rpm orbital shaking

371 or static conditions, respectively) with tryptone soya broth supplemented with 10 mM

372 glucose (TSBG) and solidified with 1.5 % agar when appropriate (Oxoid Technical No.3).

373 BHI was supplied by Becton, Dickinson and Company, Franklin Lakes, NJ. TSB and agar

374 was supplied by Oxoid Inc., Ontario, Canada. Metals for supplementation were added during

375 medium preparation. These metals and the chelator 2,2'dipyridyl were supplied by Sigma

376 Aldrich, St Louis, MO, USA.

377 **Biofilm Assay.** Bacterial cultures were normalized as described above and inoculated at 1.6-

378 3.2x10^6 CFU/200µl microtiter well in TSBG in a 96-well flat bottom transparent microtiter

379 plate (Thermo Scientific, Waltman, MA, USA), and incubated at 37°C under static

380 conditions. Uninoculated media controls with metals supplemented to the highest

381 concentration relevant to the assay were included to check for supplemented metal

382 precipitation. Supernatants were discarded and the microtitre plate washed twice with PBS.

383 To stain surface adherent bacteria, 200 µl of crystal violet solution at 0.1% w/v (Sigma-

384 Aldrich, St Louis, MO, USA) was added to each well and incubated at 4 ^{o}C for 30 minutes.

385 This solution was discarded and the microtitre plate washed twice with PBS followed by

386 crystal violet solubilization with 200 µl per well ethanol-acetone (4:1) for 45 minutes at room

387 temperature. The intensity of crystal violet staining was measured by absorbance at OD_{595nm}

388   using a Tecan Infinite 200 PRO spectrophotometer (Tecan Group Ltd., Männedorf,

389   Switzerland).

390   **Flow Cell Biofilm Assay.** Flow cell biofilm studies were performed as previously described

391   with minor modifications (61). Bacterial cultures were normalized to $2\text{-}4\times10^6$ CFU/ml in PBS

392   and 250 µl of this stock injected through the Stovall flow cell system inlet silicon tube

393   connected to the flow cell chamber. This inoculation was performed when the system flow

394   was halted by clamping both the inlet and outlet silicon tubes. The chamber was inverted for

395   one hour to facilitate bacterial adherence to the glass slide surface. The flow cell system was

396   then reset, unclamped, and the medium feed was set to 4.5 ml/hr.

397   **Transposon Library Screen.** The cryogenically stocked, 96-well format *E. faecalis* OG1RF

398   mariner transposon library consisted of 14978 individual mutants (34). This library was

399   cultured using a cryo-replicator (Adolf Kühner AG) to inoculate DeepWell blocks (Greiner

400   Bio-One) containing 1ml BHI medium for overnight incubation at 37 ^{o}C with shaking at 220

401   rpm. Cultures were normalized to OD_{600nm} 0.1 ($2\text{-}4\times10^8$ CFU/ml) in PBS with the Tecan

402   Infinite® 200 PRO spectrophotometer (Tecan Group Ltd., Switzerland) using a 96 well

403   microtiter plate. The primary screen of the library was performed by inoculating a microtitre

404   well with $1.6\text{-}3.2\times10^6$ CFU/200µl in TSBG medium supplemented with 2 mM $FeCl_3$. The

405   microtitre plates were then incubated at 37 °C, statically, inside a moistened chamber to

406   prevent evaporation of media. Biofilm was quantified by crystal violet staining as described

407   above. Mutants with either reduction or further enhancement of biofilm signal compared to

408   wild type controls were then validated using two independent biological replicates for each

409   mutant in TSBG biofilm assays. This primary validation was followed by a planktonic

410   growth validation in TSBG and TSBG medium supplemented with 2 mM $FeCl_3$. A secondary

411   validation using three independent biological replicates for each mutant was performed in

412   biofilm assays with TSBG and TSBG medium supplemented with 2 mM $FeCl_3$ to eliminate

413   any mutants exhibiting defects in biofilm formation under normal conditions.

414   **Mapping Tn Insertions.** gDNA was extracted using the Wizard® Genomic DNA

415   Purification Kit (Promega) from transposon mutants that were not originally mapped. The

416   gDNA quantified and assessed for nucleic acid quality by Qubit High Sensitive dsDNA assay

417   (Invitrogen) and NanoDrop. Sequencing was performed using an Illumina MiSeq. *de novo*

418   reads were assembled using CLC Genomics Workbench version 8.0 and *E. faecalis* OG1RF

419   as a template. The Tn insertion site was identified by BLAST using the mariner transposon

420   sequence and identification of the flanking genomic sequence. Transposon mutant strains

421   were named to include library location information, gene name or intergenic information,

422   followed by "TnMar". For example, (4.2A1 F1)10589:TnMar indicates the transposon

423   mutant for OG1RF_10589 located in block 4.2A1 of the library in position F1 of the

424   microtitre plate.

425   **Electrochemical Setup and Analysis.** Screen printed electrodes (SPE) (model DRP-C110;

426   DropSens, Spain) consisting of a carbon working electrode, carbon counter electrode, and

427   silver reference electrode were controlled by a multichannel potentiostat (Bio-Logic, France)

428   in an electrochemical cell of 9 ml working volume sealed with a Teflon cap.

429   Chronocoulometry was used to characterize the electrochemical activity of live microbial

430   cultures by measuring the charge passed over the course of growth, with the total charge in

431   mC at 40 hr used for comparison. During chronocoulometry, the working electrode was

432   poised at 200 mV vs the silver pseudoreference electrode of the SPE. This potential was

433   chosen as it is high enough to re-oxidise the reduced iron, while being low enough to avoid

434   damaging the bacteria. By applying a set potential to an electrode acting as an electron

435   acceptor, the extracellular current generated can be tracked with time, the integral of which

436   represents the total charge passed. By looking at the charge passed at a fixed time, the

437 electroactivity of a culture/mutant etc. can be established. Bacterial stocks of $2\text{-}4\times10^8$ CFU/ml

438 for electrochemical experiments were prepared as described above, and electrochemical cells

439 inoculated to $2\text{-}4\times10^5$ CFU/ml. All electrochemical experiments were conducted at 37 ^{o}C

440 using TSBG medium supplemented with 2 mM $FeCl_3$ unless otherwise stated. The iron

441 chelator, 2,2□dipyridyl (Sigma Aldrich, USA), was spiked in selected experiments to quench

442 EET.

443 **Thin-section Transmission Electron Microscopy (TEM).** Biofilms were grown using the

444 flow cell protocol or the standard biofilm protocol described, but with the latter using a 6-

445 well plate. The flow cell biofilm was resuspended in a 2 % paraformaldehyde-2.5 %

446 glutaraldehyde solution (Polysciences Inc., Warrington, PA) in 100 mM PBS (pH 7.4) for 1

447 hr at room temperature. The samples were then embedded in 2 % low-melt agarose, washed

448 in PBS and post-fixed in 1 % osmium tetroxide for 1 hr. Samples were rinsed extensively in

449 distilled water (dH_2O) prior to *en bloc* staining with 1 % aqueous uranyl acetate (Ted Pella,

450 Inc., Redding, CA, USA) for 1 hr. Following several rinses in dH_2O, samples were

451 dehydrated in a graded series of ethanol and embedded in Eponate 12 resin (Ted Pella, Inc.,

452 Redding, CA, USA). Sections of 95 nm were cut with a Leica Ultracut UCT ultramicrotome

453 (Leica Microsystems, Inc., Bannockburn, IL, USA), stained with uranyl acetate and lead

454 citrate, and viewed on a JEOL 1200 EX transmission electron microscope (JEOL USA, Inc.,

455 Peabody, MA, USA).

456 **Energy-dispersive X-ray spectroscopy (EDS) TEM**

457 Samples were prepared as described above for TEM and viewed on an aberration-corrected

458 JEOL ARM 200 cold field-emission gun transmission electron microscope in high-angle

459 annular dark-field scanning transmission (HAADF STEM) mode using spot size 6. The

460 sample was held in a JEOL Be double tilt holder tilted by about 12 ° towards the X-ray

461   detector. STEM images were collected using a JEOL annular dark-field detector on a Gatan

462   Digiscan with 2048×2048 pixels and a dwell time of 10 µs. Energy dispersive X-ray maps

463   were collected using an Oxford Aztec system with a 0.7 sr collection solid angle by scanning

464   the beam with multiple frames over a period of about 5 minutes at a resolution of 512×512

465   pixels.

466   **Confocal Laser Scanning Microscopy and 3D Reconstruction.** Biofilm morphology,

467   biovolume, and cell distribution were analyzed by CLSM directly from flow cell chamber

468   glass microscope slides at three separate locations (inlet, middle and outlet areas) with 3

469   individual Z-stack images per technical replicate. Images were acquired using LSM780

470   confocal microscope (Zeiss, Germany) equipped with 20x/0.8 Plan-Apochromat objective

471   and controlled by ZEN software. Samples were illuminated with a 488 nm Argon laser line

472   and the GFP emitted fluorescence was collected in the 507-535 nm range. Optical sections

473   (425x425 µm) were collected every 5 µm through the entire biofilm thickness and signal

474   from each section was averaged 2-4 times. Fiji software (62) was used for further processing

475   (levels adjustment, stack reslice). For the 3D biofilm reconstructions, optical slices (85x85

476   µm) were acquired with 63x/1.4 Plan-Apochromat oil immersion lens every 0.3µm through

477   entire biofilm thickness or until loss of the fluorescence signal (due to light scattering,

478   absorption, and possible fluorescence quenching of thick iron-supplemented biofilms). The

479   center of mass for each cell in 3D space was found using MosaicSuite for Fiji (63), then

480   coordinates were filtered in R (64). To visualize the biofilm matrix and spatial organization

481   coordinates were plotted as spheres with cell-size diameter and color coded Z-depth.

482   **Inductively Coupled Plasma Mass Spectroscopy (ICP-MS).** *E. faecalis* cultures were

483   prepared as previously described with minor modifications (65). Overnight cultures were

484   normalized as described above and 1-2x10^5 CFU/well was inoculated into DeepWell blocks

485   (Greiner Bio-One) containing 2 ml TSBG medium and incubated overnight at 37 ^{o}C under

486   static conditions. Three biological replicates with five technical replicates were prepared for

487   each *E. faecalis* strain and, following incubation, the technical replicates were pooled prior to

488   preparation for ICP-MS. Harvested cell pellets were washed with 10 mM EDTA (Ambion^{TM}

489   Thermofisher Scientific, USA) prepared in LC-MS grade dH$_2$O (Sigma Aldrich, St Louis,

490   MO, USA) and washed three times with LC-MS grade dH$_2$0. Cells were then concentrated to

491   2-4x10^8 CFU/ml in LC-MS grade dH$_2$O. Each cell pellet was digested in 500 µl of 69 %

492   nitric acid and 250 µl of 31 % hydrogen peroxide. Following sample digestion, all the

493   samples were diluted with LC-MS grade dH$_2$0 to a 2 % (w/v) nitric acid concentration in the

494   final solution.

495   An Agilent 7700 series model ICP-MS system (Agilent, Santa Clara, CA, USA) was used for

496   simultaneous determination of selected elements [Mg, Al, P, K, Ca, V, Cr, Mn, Fe, Co, Ni,

497   Cu, Zn] in prepared *E. faecalis* samples. Prior to sample measurement and quantification,

498   stock solutions of a multi-element calibration standard (Inorganic Ventures, VA, USA) were

499   serially diluted (0 µg/L to 1000 µg/L) and run on the system. For each measurement

500   (standards, samples, blanks, and quality controls), addition of internal standard (Sc; 100

501   mg/L, Agilent, USA) was performed to correct for physical matrix effects. Blanks were

502   determined together with samples for every run and the mean of three runs was determined

503   for each sample. Full quantitative analysis was performed against calibration standards for

504   each element. Quality control samples (multi-element calibration solution; 100 µL) were

505   inserted and run at regular intervals during the experiment to ensure reliability of the data and

506   to eliminate signal drift or interference.

507   For statistical analysis, 10 metals were measured for 22 phenotypes (*E. faecalis* OG1RF wild

508   type and 21 mutants) in three nutrient conditions, with 3 biological replicates for each mutant

509   and in each condition. During the ICP-MS run, 3 technical replicates were measured from

510   each sample, which were then averaged and used for statistical analysis. The concentration of

511   the metals in a blank control (500 µl of 69% nitric acid and 250 µl of 31% hydrogen

512   peroxide) was subtracted from the concentration of metals in the samples. Metals whose

513   levels were below the detection limit were coded as not detected. For statistical analysis,

514   metal concentrations were normalized using log base 10 transformation. To test differences

515   between the metal levels in mutants and the control in each nutrient condition, Welch's two

516   sample t-tests were performed in R using the t.test function, with correction for multiple

517   comparisons made using the Benjamini-Hochberg procedure.

518 **Author Contributions**

519 D.K. conceptualized the study. D.K., L.N.L., E.M., and K.A.K. designed the experiments,

520 analyzed data, and prepared the manuscript. D.K. and L.N.L. performed biofilm experiments

521 and analyzed data. A.M. analyzed confocal data and generated 3D reconstruction models.

522 D.K. and S.P. performed the ICP-MS experiments. S.U. and R.B.H.W. analyzed

523 metabolomics data. D.K., L.E.D., L.N.L., and E.M. performed the electrochemistry

524 experiments and analyzed data. L.N.L and C.B. performed EDS TEM. J.D. and G.D.

525 provided the transposon library. All authors reviewed the manuscript.

Acknowledgments

References

1. Hufnagel M, Liese C, Loescher C, Kunze M, Proempeler H, Berner R, Krueger M. 2007. Enterococcal colonization of infants in a neonatal intensive care unit: associated predictors, risk factors and seasonal patterns. BMC Infect Dis 7:107.

2. Sekirov I, Russell SL, Antunes LC, Finlay BB. 2010. Gut microbiota in health and disease. Physiol Rev 90:859-904.

3. Flemming HC, Wingender J, Szewzyk U, Steinberg P, Rice SA, Kjelleberg S. 2016. Biofilms: an emergent form of bacterial life. Nat Rev Microbiol 14:563-75.

4. Rice LB. 2005. Antibiotics and gastrointestinal colonization by vancomycin-resistant enterococci. Eur J Clin Microbiol Infect Dis 24:804-14.

5. Rice LB, Hutton-Thomas R, Lakticova V, Helfand MS, Donskey CJ. 2004. Beta-lactam antibiotics and gastrointestinal colonization with vancomycin-resistant enterococci. J Infect Dis 189:1113-8.

6. Trajkovska-Dokic E, Kaftandzieva A, Stojkovska S, Kuzmanovska A, Panovski N. 2015. Gastrointestinal Colonization with Vancomycin-Resistant Enterococci In Hospitalized and Outpatients. Open Access Maced J Med Sci 3:7-11.

7. Bowler PG, Duerden BI, Armstrong DG. 2001. Wound microbiology and associated approaches to wound management. Clin Microbiol Rev 14:244-69.

8. Flores-Mireles AL, Walker JN, Caparon M, Hultgren SJ. 2015. Urinary tract infections: epidemiology, mechanisms of infection and treatment options. Nat Rev Microbiol doi:10.1038/nrmicro3432.

9. Nallapareddy SR, Singh KV, Sillanpaa J, Garsin DA, Hook M, Erlandsen SL, Murray BE. 2006. Endocarditis and biofilm-associated pili of Enterococcus faecalis. J Clin Invest 116:2799-807.

567   10.   Hamada Y, Magarifuchi H, Oho M, Kusaba K, Nagasawa Z, Fukuoka M, Yamakuchi
568   H, Urakami T, Aoki Y. 2015. Clinical features of enterococcal bacteremia due to
569   ampicillin-susceptible and ampicillin-resistant enterococci: An eight-year
570   retrospective comparison study. J Infect Chemother 21:527-30.

571   11.   Baureder M, Hederstedt L. 2012. Genes important for catalase activity in
572   Enterococcus faecalis. PLoS One 7:e36725.

573   12.   Frankenberg L, Brugna M, Hederstedt L. 2002. Enterococcus faecalis heme-
574   dependent catalase. J Bacteriol 184:6351-6.

575   13.   Weinberg ED. 1997. The Lactobacillus anomaly: total iron abstinence. Perspect Biol
576   Med 40:578-83.

577   14.   Bruyneel B, Vandewoestyne M, Verstraete W. 1989. Lactic-Acid Bacteria -
578   Microorganisms Able to Grow in the Absence of Available Iron and Copper.
579   Biotechnology Letters 11:401-406.

580   15.   Marcelis JH, den Daas-Slagt HJ, Hoogkamp-Korstanje JA. 1978. Iron requirement
581   and chelator production of staphylococci, Streptococcus faecalis and
582   enterobacteriaceae. Antonie van Leeuwenhoek 44:257-67.

583   16.   Archibald F. 1986. Manganese: its acquisition by and function in the lactic acid
584   bacteria. Crit Rev Microbiol 13:63-109.

585   17.   Verneuil N, Maze A, Sanguinetti M, Laplace JM, Benachour A, Auffray Y, Giard JC,
586   Hartke A. 2006. Implication of (Mn)superoxide dismutase of Enterococcus faecalis in
587   oxidative stress responses and survival inside macrophages. Microbiology 152:2579-
588   89.

589   18.   Riboulet E, Verneuil N, La Carbona S, Sauvageot N, Auffray Y, Hartke A, Giard JC.
590   2007. Relationships between oxidative stress response and virulence in Enterococcus
591   faecalis. Journal of molecular microbiology and biotechnology 13:140-6.

592   19.   Andrews SC, Robinson AK, Rodriguez-Quinones F. 2003. Bacterial iron homeostasis.

593   FEMS Microbiol Rev 27:215-37.

594   20.   Alexander J, Kowdley KV. 2009. HFE-associated hereditary hemochromatosis. Genet

595   Med 11:307-13.

596   21.   Cao A, Galanello R. 2010. Beta-thalassemia. Genet Med 12:61-76.

597   22.   Lee T, Clavel T, Smirnov K, Schmidt A, Lagkouvardos I, Walker A, Lucio M,

598   Michalke B, Schmitt-Kopplin P, Fedorak R, Haller D. 2016. Oral versus intravenous

599   iron replacement therapy distinctly alters the gut microbiota and metabolome in

600   patients with IBD. Gut doi:10.1136/gutjnl-2015-309940.

601   23.   Kopani M, Miglierini M, Lancok A, Dekan J, Caplovicova M, Jakubovsky J, Boca R,

602   Mrazova H. 2015. Iron oxides in human spleen. Biometals 28:913-28.

603   24.   Flahaut S, Laplace JM, Frere J, Auffray Y. 1998. The oxidative stress response in

604   Enterococcus faecalis: relationship between H2O2 tolerance and H2O2 stress

605   proteins. Lett Appl Microbiol 26:259-64.

606   25.   Keogh D, Tay WH, Ho YY, Dale JL, Chen S, Umashankar S, Williams RB, Chen SL,

607   Dunny GM, Kline KA. 2016. Enterococcal Metabolite Cues Facilitate Interspecies

608   Niche Modulation and Polymicrobial Infection. Cell Host Microbe 20:493-503.

609   26.   Dale JL, Cagnazzo J, Phan CQ, Barnes AM, Dunny GM. 2015. Multiple roles for

610   Enterococcus faecalis glycosyltransferases in biofilm-associated antibiotic resistance,

611   cell envelope integrity, and conjugative transfer. Antimicrob Agents Chemother

612   59:4094-105.

613   27.   Seneviratne CJ, Yip JW, Chang JW, Zhang CF, Samaranayake LP. 2013. Effect of

614   culture media and nutrients on biofilm growth kinetics of laboratory and clinical

615   strains of Enterococcus faecalis. Arch Oral Biol 58:1327-34.

616   28.   Barnes AM, Ballering KS, Leibman RS, Wells CL, Dunny GM. 2012. Enterococcus

617   faecalis produces abundant extracellular structures containing DNA in the absence of

618   cell lysis during early biofilm formation. MBio 3:e00193-12.

619   29.   Thomas VC, Hiromasa Y, Harms N, Thurlow L, Tomich J, Hancock LE. 2009. A

620   fratricidal mechanism is responsible for eDNA release and contributes to biofilm

621   development of Enterococcus faecalis. Mol Microbiol 72:1022-36.

622   30.   Guiton PS, Hung CS, Kline KA, Roth R, Kau AL, Hayes E, Heuser J, Dodson KW,

623   Caparon MG, Hultgren SJ. 2009. Contribution of autolysin and Sortase a during

624   Enterococcus faecalis DNA-dependent biofilm development. Infect Immun 77:3626-

625   38.

626   31.   O'Toole GA. 2011. Microtiter dish biofilm formation assay. J Vis Exp

627   doi:10.3791/2437.

628   32.   Borisov VB, Gennis RB, Hemp J, Verkhovsky MI. 2011. The cytochrome bd

629   respiratory oxygen reductases. Biochim Biophys Acta 1807:1398-413.

630   33.   Foster AW, Osman D, Robinson NJ. 2014. Metal preferences and metallation. J Biol

631   Chem 289:28095-103.

632   34.   Kristich CJ, Nguyen VT, Le T, Barnes AM, Grindle S, Dunny GM. 2008.

633   Development and use of an efficient system for random mariner transposon

634   mutagenesis to identify novel genetic determinants of biofilm formation in the core

635   Enterococcus faecalis genome. Appl Environ Microbiol 74:3377-86.

636   35.   Shi L, Dong H, Reguera G, Beyenal H, Lu A, Liu J, Yu HQ, Fredrickson JK. 2016.

637   Extracellular electron transfer mechanisms between microorganisms and minerals.

638   Nat Rev Microbiol doi:10.1038/nrmicro.2016.93.

639   36.   Logan BE. 2009. Exoelectrogenic bacteria that power microbial fuel cells. Nat Rev

640   Microbiol 7:375-81.

641 37. Embree M, Qiu Y, Shieu W, Nagarajan H, O'Neil R, Lovley D, Zengler K. 2014. The
642   iron stimulon and fur regulon of Geobacter sulfurreducens and their role in energy
643   metabolism. Appl Environ Microbiol 80:2918-27.

644 38. Yang Y, Harris DP, Luo F, Wu L, Parsons AB, Palumbo AV, Zhou J. 2008.
645   Characterization of the Shewanella oneidensis Fur gene: roles in iron and acid
646   tolerance response. BMC Genomics 9 Suppl 1:S11.

647 39. Okamoto A, Nakamura R, Hashimoto K. 2011. In-vivo identification of direct
648   electron transfer from Shewanella oneidensis MR-1 to electrodes via outer-membrane
649   OmcA-MtrCAB protein complexes. Electrochimica Acta 56:5526-5531.

650 40. Marsili E, Rollefson JB, Baron DB, Hozalski RM, Bond DR. 2008. Microbial biofilm
651   voltammetry: direct electrochemical characterization of catalytic electrode-attached
652   biofilms. Appl Environ Microbiol 74:7329-37.

653 41. von Canstein H, Ogawa J, Shimizu S, Lloyd JR. 2008. Secretion of flavins by
654   Shewanella species and their role in extracellular electron transfer. Appl Environ
655   Microbiol 74:615-23.

656 42. Wang Y, Kern SE, Newman DK. 2010. Endogenous phenazine antibiotics promote
657   anaerobic survival of Pseudomonas aeruginosa via extracellular electron transfer. J
658   Bacteriol 192:365-9.

659 43. Schröder U, Harnisch F, Angenent LT. 2015. Microbial electrochemistry and
660   technology: terminology and classification. Energy & Environmental Science 8:513-
661   519.

662 44. Aeschbacher M, Sander M, Schwarzenbach RP. 2010. Novel electrochemical
663   approach to assess the redox properties of humic substances. Environ Sci Technol
664   44:87-93.

665 45. Kim E, Gordonov T, Bentley WE, Payne GF. 2013. Amplified and in Situ Detection
666   of Redox-Active Metabolite Using a Biobased Redox Capacitor. Analytical
667   Chemistry 85:2102-2108.

668 46. Abbaspour N, Hurrell R, Kelishadi R. 2014. Review on iron and its importance for
669   human health. J Res Med Sci 19:164-74.

670 47. Lebreton F, Willems RJL, Gilmore MS. 2014. Enterococcus Diversity, Origins in
671   Nature, and Gut Colonization. *In* Gilmore MS, Clewell DB, Ike Y, Shankar N (ed),
672   Enterococci: From Commensals to Leading Causes of Drug Resistant Infection,
673   Boston.

674 48. Kim GT, Hyun MS, Chang IS, Kim HJ, Park HS, Kim BH, Kim SD, Wimpenny JW,
675   Weightman AJ. 2005. Dissimilatory Fe(III) reduction by an electrochemically active
676   lactic acid bacterium phylogenetically related to Enterococcus gallinarum isolated
677   from submerged soil. J Appl Microbiol 99:978-87.

678 49. Zhang E, Cai Y, Luo Y, Piao Z. 2014. Riboflavin-shuttled extracellular electron
679   transfer from Enterococcus faecalis to electrodes in microbial fuel cells. Can J
680   Microbiol 60:753-9.

681 50. Lechardeur D, Cesselin B, Fernandez A, Lamberet G, Garrigues C, Pedersen M,
682   Gaudu P, Gruss A. 2011. Using heme as an energy boost for lactic acid bacteria. Curr
683   Opin Biotechnol 22:143-9.

684 51. Richardson DJ. 2000. Bacterial respiration: a flexible process for a changing
685   environment. Microbiology 146 (Pt 3):551-71.

686 52. Winstedt L, Frankenberg L, Hederstedt L, von Wachenfeldt C. 2000. Enterococcus
687   faecalis V583 contains a cytochrome bd-type respiratory oxidase. J Bacteriol
688   182:3863-6.

689 53. Pedersen MB, Gaudu P, Lechardeur D, Petit MA, Gruss A. 2012. Aerobic respiration

690   metabolism in lactic acid bacteria and uses in biotechnology. Annu Rev Food Sci

691   Technol 3:37-58.

692 54. Rezaiki L, Lamberet G, Derre A, Gruss A, Gaudu P. 2008. Lactococcus lactis

693   produces short-chain quinones that cross-feed Group B Streptococcus to activate

694   respiration growth. Mol Microbiol 67:947-57.

695 55. Miethke M, Marahiel MA. 2007. Siderophore-based iron acquisition and pathogen

696   control. Microbiol Mol Biol Rev 71:413-51.

697 56. Vebo HC, Snipen L, Nes IF, Brede DA. 2009. The transcriptome of the nosocomial

698   pathogen Enterococcus faecalis V583 reveals adaptive responses to growth in blood.

699   PLoS ONE 4:e7660.

700 57. Vebo HC, Solheim M, Snipen L, Nes IF, Brede DA. 2010. Comparative genomic

701   analysis of pathogenic and probiotic Enterococcus faecalis isolates, and their

702   transcriptional responses to growth in human urine. PLoS ONE 5:e12489.

703 58. Waldron KJ, Robinson NJ. 2009. How do bacterial cells ensure that metalloproteins

704   get the correct metal? Nat Rev Microbiol 7:25-35.

705 59. Dunny GM, Brown BL, Clewell DB. 1978. Induced cell aggregation and mating in

706   Streptococcus faecalis: evidence for a bacterial sex pheromone. Proc Natl Acad Sci U

707   S A 75:3479-83.

708 60. Debroy S, van der Hoeven R, Singh KV, Gao P, Harvey BR, Murray BE, Garsin DA.

709   2012. Development of a genomic site for gene integration and expression in

710   Enterococcus faecalis. J Microbiol Methods 90:1-8.

711 61. Paganelli FL, Willems RJ, Jansen P, Hendrickx A, Zhang X, Bonten MJ, Leavis HL.

712   2013. Enterococcus faecium biofilm formation: identification of major autolysin

713   AtlAEfm, associated Acm surface localization, and AtlAEfm-independent

714   extracellular DNA Release. MBio 4:e00154.

715 62. Schindelin J, Arganda-Carreras I, Frise E, Kaynig V, Longair M, Pietzsch T,

716   Preibisch S, Rueden C, Saalfeld S, Schmid B, Tinevez JY, White DJ, Hartenstein V,

717   Eliceiri K, Tomancak P, Cardona A. 2012. Fiji: an open-source platform for

718   biological-image analysis. Nat Methods 9:676-82.

719 63. Sbalzarini IF, Koumoutsakos P. 2005. Feature point tracking and trajectory analysis

720   for video imaging in cell biology. J Struct Biol 151:182-95.

721 64. Team RC. 2016. R: A Language and Environment for Statistical Computing.

722 65. Rolfe MD, Rice CJ, Lucchini S, Pin C, Thompson A, Cameron AD, Alston M,

723   Stringer MF, Betts RP, Baranyi J, Peck MW, Hinton JC. 2012. Lag phase is a distinct

724   growth phase that prepares bacteria for exponential growth and involves transient

725   metal accumulation. J Bacteriol 194:686-701.

726

727

728 **Figures**

729

730 **Figure 1:** *E. faecalis* **flow cell biofilms in iron supplemented media.** (**a**) CSLM images at

731 8, 12, and 18 hr for normal (10 % TSBG) and supplemented (10% TSBG plus 0.2 mM

732 FeCl$_3$). Selected optical sections at the indicated depths are followed by representative lateral

733 view in YZ at the right of each image set. Scale bar 100 μm. (**b**) 3D reconstructions of high

734 magnification CLSM stacks of *E. faecalis* flow cell biofilms grown in normal or

735 supplemented medium for 18 hr at 37 ^{o}C or 120 hr at 22 ^{o}C. Biofilm depth is color-coded as

736 indicated on z-depth scale (0 to 24 μm) and the lateral box dimensions are 85 x 85 μm (20

737 μm between ticks).

738

739 **Figure 2: Electron micrographs of the** *E. faecalis* **biofilm matrix with iron**

740 **supplementation.** Representative images from TEM of *E. faecalis* biofilm from flow cell in

741 normal 10 % TSBG (**a**, **b**, **c**) or 10 % TSBG supplemented with 0.2 mM FeCl$_3$ (**d**, **e**, **f**). In a-f,

742 scale bars represent 2 μm (black) and 0.5 μm (white), and red arrows highlight examples of

743 electron dense particles. The biofilm matrix from biofilms grown in normal media (g, h, i) or

744 with iron supplementation (j, k, l) was examined by HAADF STEM and EDS mapping at

745 300,000x magnification: HAADF STEM (g, j), iron EDS map (h, k), and merged EDS-STEM

746 images (i, l) are shown at 300,000x magnification. Scale bars in g-l represent 1 μm. The EDS

747 spectra for iron, corresponding to the images are shown in m.

748

749

750   **Figure 3: *E. faecalis* biofilm growth under metal supplementation.** (**a**) Time course of *E.*

751   *faecalis* biofilm growth in TSBG supplemented with $FeCl_3$. (**b**) *E. faecalis* biofilm growth at

752   120hr in TSBG supplemented with metals as indicated. (**c**) ICP-MS analysis of *E. faecalis*

753   grown in TSBG (normal) and TSBG supplemented with 2mM $FeCl_3$ (Supplemented). (**a** and

754   **b**) Data at each time point or metal supplement represents an independent experiment, with

755   the data merged for representation. (**a-c**) n = 3 biological replicates. Statistical significance

756   was determined by two-way ANOVA with Tukey's test for multiple comparisons, n = 3 with

757   four technical replicates, * $P \leq 0.05$, ** $P \leq 0.01$, *** $P \leq 0.001$, **** $P \leq 0.0001$. (**a**) Statistical

758   analysis was calculated with time set as a 'repeated measure'. (**a**, **b**, **c**) error bars represent

759   standard deviation (SD) from the mean.

760

761   **Figure 4: Extracellular electron transfer in *E. faecalis* biofilm.** (**a**) Chronocoulometry

762   current (Q) measurement, expressed in milicoulombs (mC), of *E. faecalis* biofilm on a

763   screen-printed carbon mini-electrode over 40 hr in TSBG supplemented with 2mM $FeCl_3$

764   (Supplemented). Abiotic controls and media controls are indicated. Statistical significance

765   was determined by one-way ANOVA with Tukey's test for multiple comparisons, n = 3

766   biological replicates, error bars represent SD from the mean, **** $P \leq 0.0001$. (**b**)

767   Chronocoulometry of *E. faecalis* biofilm in iron supplemented medium with a chelator spike

768   (10 mM 2,2☐dipyridyl) at 7.5 hr. Representative data from four independent experiments are

769   shown, where the trend is consistent among all experiments. Statistical significance was

770   determined by a paired two-tailed t-test, error bars (light-green or -red shading) represent SD

771   from the mean, **** $P \leq 0.0001$.

772

773   **Figure 5: Fermentation and EET-dependent respiration metabolism in *E. faecalis***

774   **biofilm.** Schematic model for *E. faecalis* biofilm metabolism describing EET through DET

775   and MET mechanisms. ATP is generated by proton flow through membrane integrated ATP

776   synthases. Glycolysis and fermentation are required prior to EET-dependent respiration. This

777   generates the fermentation end-products required as substrates for dehydrogenases acting as

778   electron donors. DET occurs in the absence of heme, where extracellular iron can be reduced

779   and thereby serve as an iron sink for electrons of the respiratory electron transport chain.

780   MET occurs in the absence of heme, when iron is transported intracellularly and reduced,

781   thereafter being exported and serving as an electron mediator/shuttle.

782

783   **Figure S1: *E. faecalis* planktonic growth under metal supplementation.** (**a**) Time course

784   enumeration of *E. faecalis* planktonic growth over 24hr in TSBG and TSBG supplemented

785   with 2mM $FeCl_3$. n = 3 biological replicates, error bars represent standard deviation (SD)

786   from the mean.

787

788   **Figure S2: Metal precipitation control.** Static incubation of TSBG medium supplemented

789   with $FeCl_3$ over time. n = 2 replicates, error bars represent standard deviation (SD) from the

790   mean.

791

792   **Figure S3: Electron micrographs of the *E. faecalis* biofilm matrix in the absence or**

793   **presence of metal supplementation.** Representative images from TEM of *E. faecalis*

794   biofilm from 24 hr static biofilms grown in normal TSBG (a, e), TSBG supplemented with 2

795   mM $FeCl_3$ (b, e), or 50 uM heme (c, f). Scale bars represent 2 μm (black) and 0.5 μm (white).

796

797 **Figure S4: Transposon library screen for mutants exhibiting changes in biofilm**

798 **accumulation under iron supplementation.** (**a**) Flow chart of screen process including

799 evaluation criteria for biofilm assays. (**b-g**) Secondary validation data for mutants passing

800 primary evaluation. Light grey indicates normal medium and dark grey indicates iron

801 supplemented medium. Secondary validation bar charts represent individual experiments and

802 are separately presented, rather than being pooled, for greater clarity.

803

804 **Figure S5: Biofilm biovolume and metal-dependence of *E. faecalis* EET.** CLSM images

805 of *E. faecalis* biofilm on screen-printed electrode (SPE) at the end of chronocoulometry

806 measurements after 20 hrs growth in (**a**) normal TSBG or (**b**) TSBG supplemented with 2

807 mM $FeCl_3$. (**c**) Charge (mC) transferred from *E. faecalis* biofilm to the SPE after 20 hr in

808 normal TSBG, TSBG supplemented with 2mM $FeCl_3$, 2mM manganese chloride ($MnCl_2$), 2

809 mM magnesium sulfate ($MgSO_4$), or 50uM heme. These results were measured in glass

810 electrochemical cells willed with 11 mL growth medium. All the other parameters are the

811 same described in the Materials and Methods section. The working electrode was poised at

812 200 mV vs the silver pseudoreference electrode of the SPE.

813

814 **Table S1: Metallome of *E. faecalis* in normal and iron supplemented conditions**

815

816 **Table S2: Metallome comparison of *E. faecalis* mutants versus wild type in normal**

817 **condition**

818

819   **Table S3: Metallome comparison of *E. faecalis* mutants versus wild type in deplete**

820   **condition**

821

822   **Table S4: Metallome comparison of *E. faecalis* mutants versus wild type in**

823   **supplemented condition**
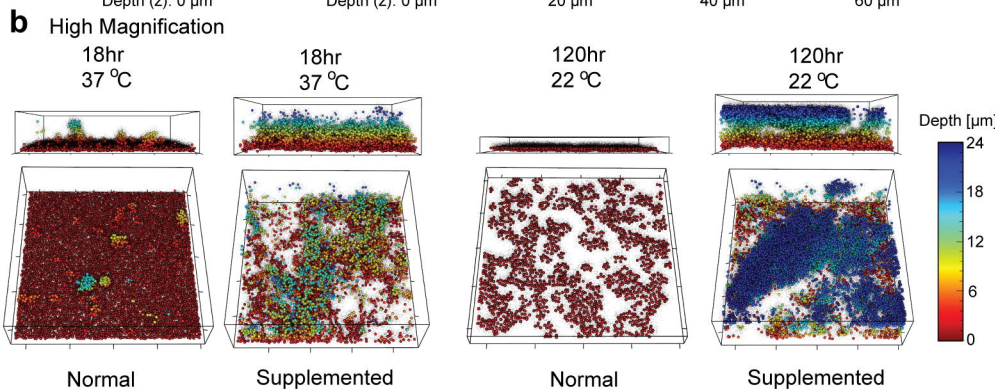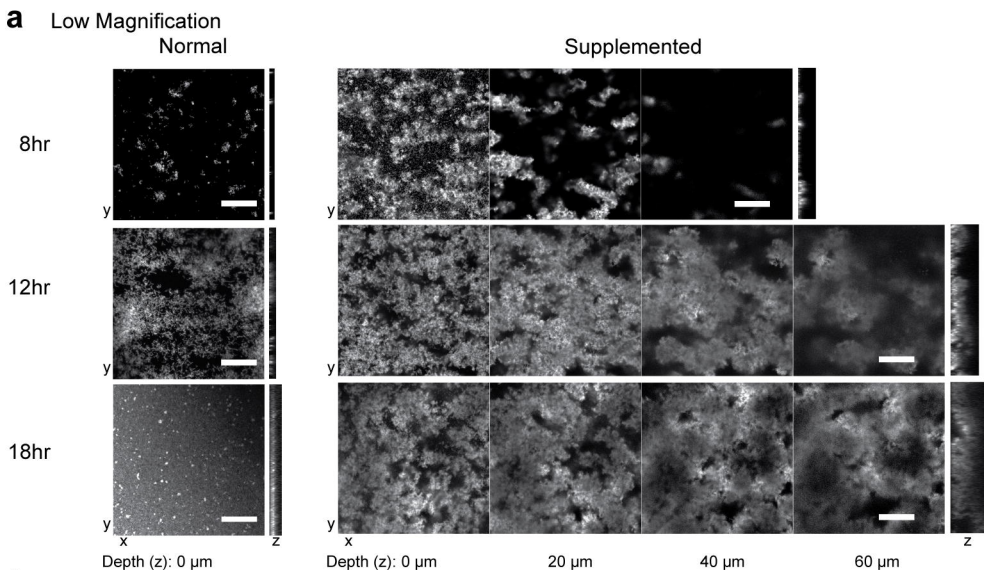
824

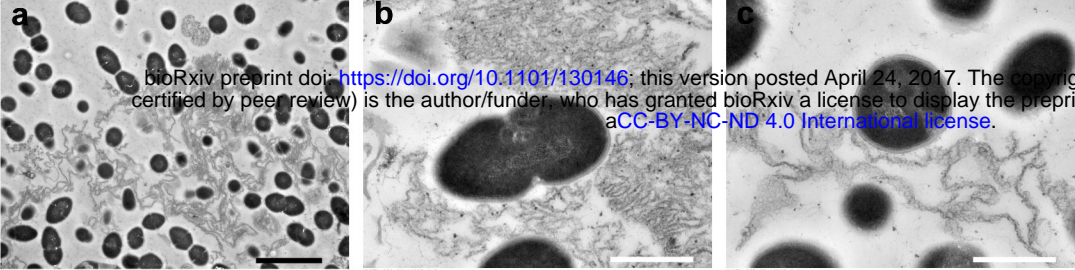825   **Table S5: *E. faecalis* mutants in deplete condition where iron was not detected**

826

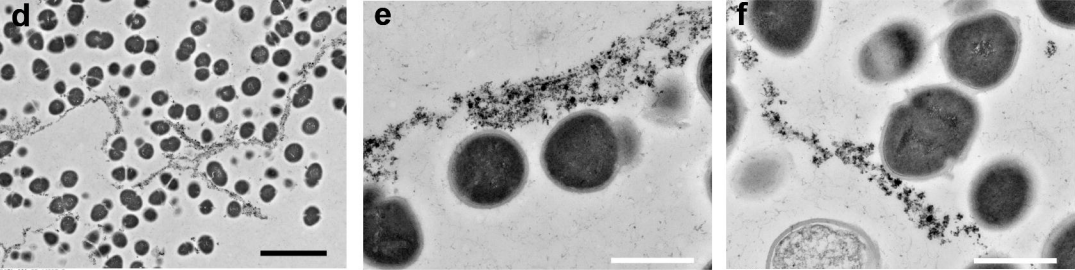827   **Table S6: *E. faecalis* components involved in iron-induced biofilm growth**
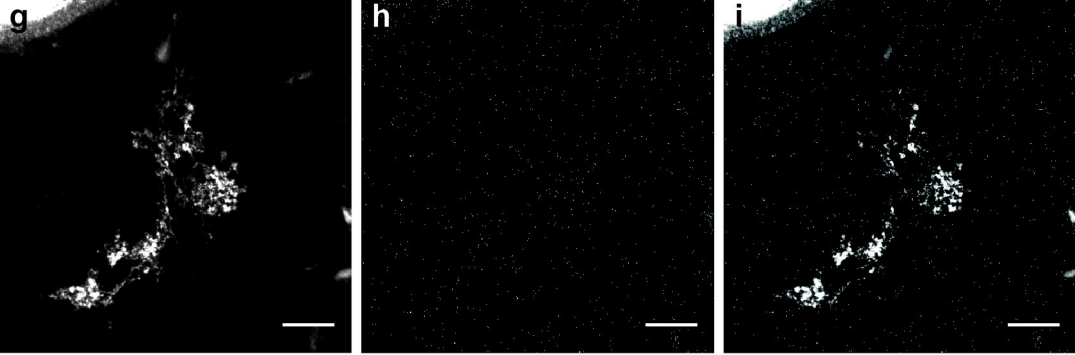
828

829

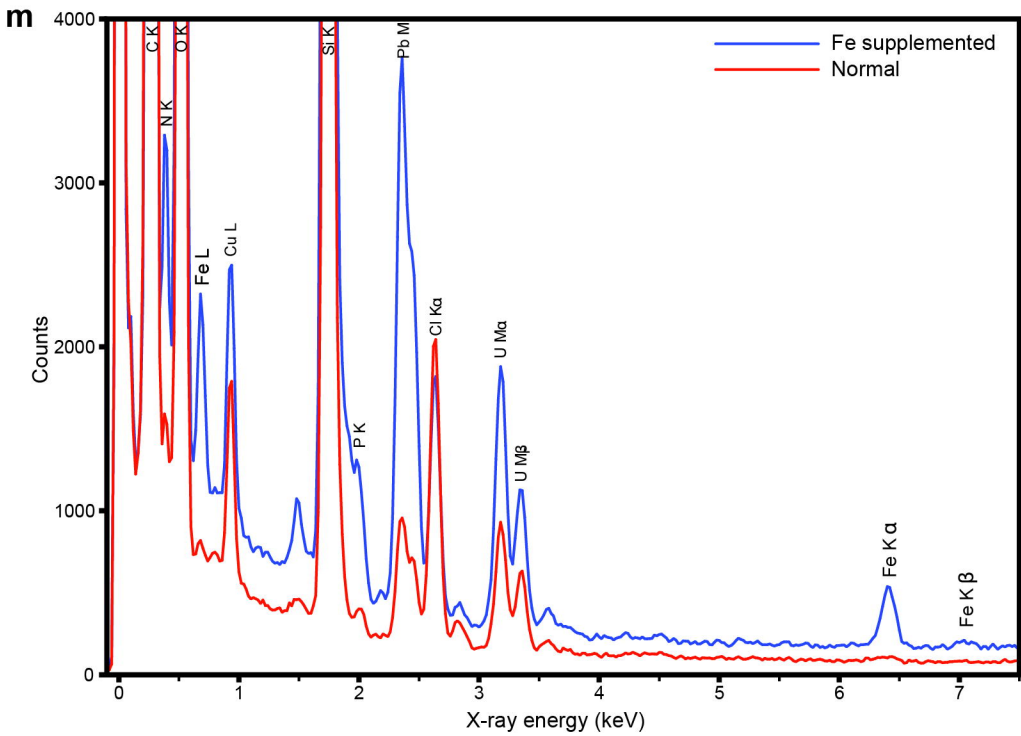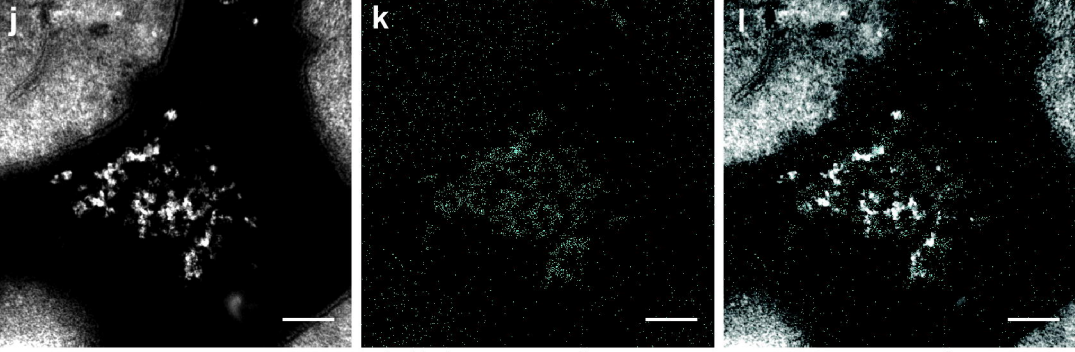**a** Low Magnification

Normal   Supplemented

8hr

12hr

18hr

Depth (z): 0 µm   Depth (z): 0 µm   20 µm   40 µm   60 µm

b High Magnification

18hr 37 °C   18hr 37 °C   120hr 22 °C   120hr 22 °C

Depth [µm]

24
18
12
6
0

Normal   Supplemented   Normal   Supplemented

Normal Media

a b c

Iron Supplemented

d e f

Normal Media

g h i

Iron Supplemented

j k l

m
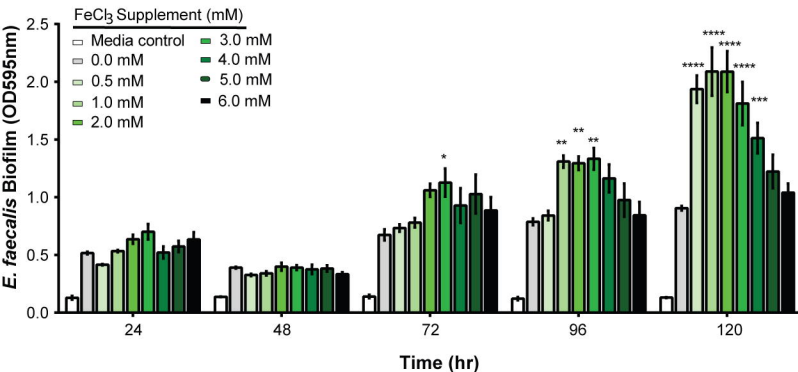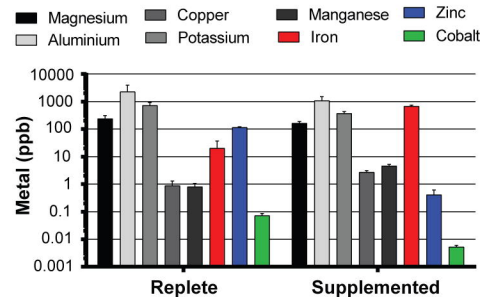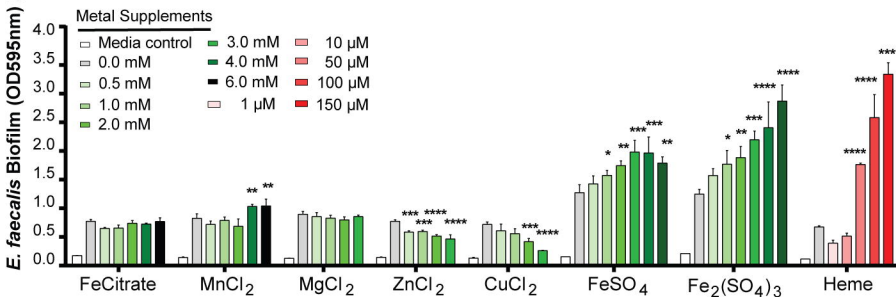
a
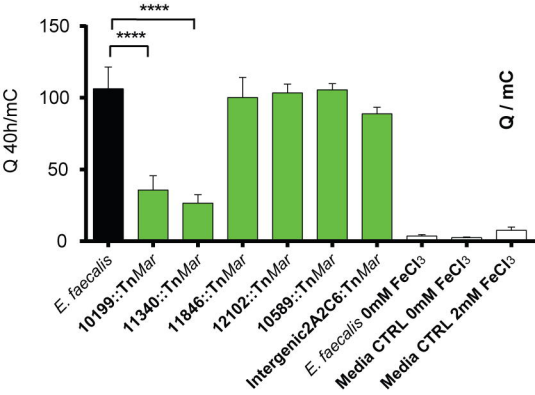
b
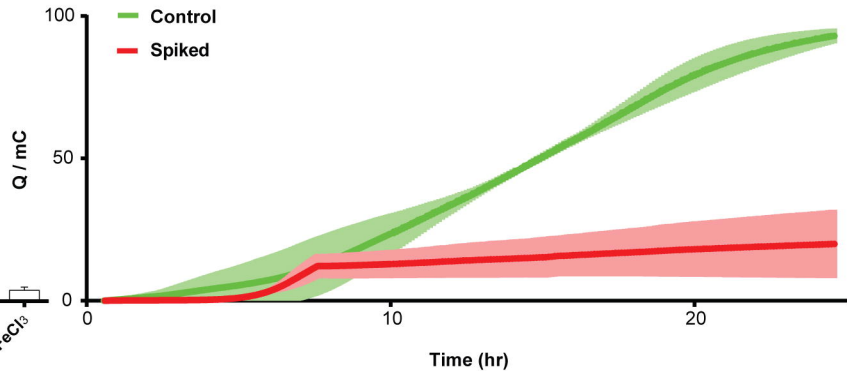
e⁻ Transport, EET & Iron Reduction

DET

MET

OUT
CM
IN

H^+

NADH Dehydrogenase
e⁻ Donor

DMQ

Cytochrome *bd*
Heme Dependent

Fe^{3+} Fe^{2+}

e⁻

H^+

NADH + H⁺   NAD⁺

O_2 H_2O

Fe^{3+} Fe^{2+}

Fe^{3+} Fe^{2+}

e⁻

H^+

NADH Dehydrogenase
e⁻ Donor

H^+

NADH + H⁺   NAD⁺

H^+

ATP Synthase

H^+

ADP + Pi   ATP

Glycolysis & Fermentation

Pyruvate → Pyruvate

2 ATP

NADH + H⁺

2 ADP + Pi

Glucose-6-Phosphate

NAD⁺ + Pi

LDH

Lactate

Glucose

Heme

Aerobic Respiration
(cytochrome *bd*)

Acetyl-Co-A's

Acetaldehyde

NADH + H⁺

ADH

NAD⁺

Ethanol

ADP + Pi   ATP

H^+

IN
CM
OUT

ATP Synthase

H^+